PROCEEDINGS OF SCIENCE

Recent results from ATLAS

Frank Winklmeier*
On behalf of the ATLAS Collaboration

European Laboratory for Particle Physics (CERN), Geneva
E-mail: frank.winklmeier@cern.ch

We review recent results of the ATLAS experiment at the Large Hadron Collider (LHC) at CERN using data collected during 7 TeV and 8 TeV proton-proton collisions, lead-lead collisions at 2.76 TeV and proton-lead collisions at 5.02 TeV center-of-mass energy. The results shown here include Standard Model measurements of the W/Z boson and top quark, most recent updates on the search for a Higgs-like particle around 125 GeV and searches for Supersymmetry. Finally, selected heavy ion results from lead-lead and proton-lead collisions are presented.

51st International Winter Meeting on Nuclear Physics
21-25 January 2013
Bormio (Italy)

*Speaker.

PoS(Bormio 2013)063

1. Introduction

The ATLAS experiment [1] is one of the four large experiments at the Large Hadron Collider (LHC) [2] at CERN. The first proton-proton collisions were recorded in 2009 and during 2010/11 ATLAS recorded data corresponding to an integrated luminosity of $5.6\,\text{fb}^{-1}$ at a centre-of-mass energy of 7 TeV. During the 2012 data taking period at 8 TeV, ATLAS recorded data corresponding to an integrated luminosity of $21.6\,\text{fb}^{-1}$ of which 96% were declared as good quality data to be used for physics analyses. Using these data ATLAS has performed a wide range of physics analyses of which some of the most recent ones are presented in these proceedings. After a brief introduction of the ATLAS detector, section 3 shows recent Standard Model physics results in top pair production and diboson physics. Section 4 and 5 present the main analyses in the search for the Standard Model Higgs boson and recent results on Supersymmetry searches, respectively. In addition, ATLAS has recorded data during lead-lead and proton-lead collisions used in heavy ion physics analyses that are shown in section 6.

2. The ATLAS detector

The ATLAS detector [1] is a multi-purpose particle physics detector with approximately forward-backward symmetric cylindrical geometry[1]. The inner tracking detector (ID) [3] covers $|\eta| < 2.5$ and consists of a silicon pixel detector, a silicon micro-strip detector, and a transition radiation tracker. The ID is surrounded by a thin superconducting solenoid providing a 2T axial magnetic field. A high-granularity lead/liquid-argon (LAr) sampling calorimeter [4] measures the energy and the position of electromagnetic showers within $|\eta| < 3.2$. LAr sampling calorimeters are also used to measure hadronic showers in the end-cap ($1.5 < |\eta| < 3.2$) and forward ($3.1 < |\eta| < 4.9$) regions (FCal), while an iron/scintillator tile calorimeter [5] measures hadronic showers in the central region ($|\eta| < 1.7$). The muon spectrometer (MS) [6] surrounds the calorimeters and consists of three large superconducting air-core toroid magnets, each with eight coils, a system of precision tracking chambers ($|\eta| < 2.7$), and fast tracking chambers for triggering. A three-level trigger system [7] selects events to be recorded for offline analysis.

3. Standard Model physics

Thanks to the large amount of recorded data together with tremendous advances in theory calculations, precision measurements of electroweak and top processes become a reality. This is important for detector calibration, understanding the backgrounds in the Higgs and beyond the Standard Model (SM) searches as well as direct searches for deviations from the SM. Figure 1 shows the summary of several SM production cross sections measured at 7 TeV and 8 TeV together with the theoretical expectations. The measurement of the top pair and ZZ production cross section are described in more detail in the following.

[1] ATLAS uses a right-handed coordinate system with its origin at the nominal interaction point. The z-axis is along the beam pipe, the x-axis points to the centre of the LHC ring and the y-axis is defined as pointing upwards. Polar coordinates (r,ϕ) are used in the transverse plane, ϕ being the azimuthal angle around the beam pipe. The pseudo-rapidity η is defined as $\eta = -\ln[\tan(\theta/2)]$ where θ is the polar angle.

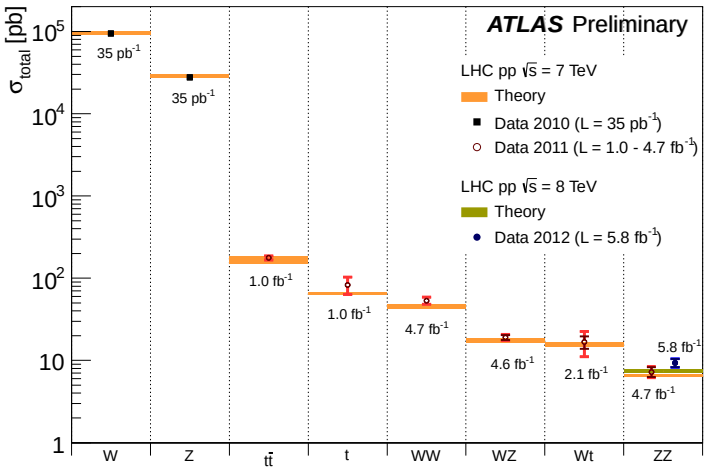

Figure 1: Summary of several Standard Model total production cross section measurements compared to the corresponding theoretical expectations [8]. The top quark pair production cross-section is based on a statistical combination of measurements in the single-lepton, dilepton and all-hadronic channels using up to $1.02\,\mathrm{fb}^{-1}$ of data. The single-top measurement uses $0.7\,\mathrm{fb}^{-1}$ of data, while the WZ measurement uses $1.02\,\mathrm{fb}^{-1}$. The WW and ZZ measurements were made with the full 2011 dataset. The dark error bar represents the statistical uncertainly. The red error bar represents the full uncertainty, including systematics and luminosity uncertainties. All theoretical expectations were calculated at NLO or higher.

3.1 Top pair production

The top quark is the heaviest fermion in the SM and has thus the largest Yukawa coupling with the Higgs boson. It may also couple to other heavy particles predicted by extensions of the SM. Additional processes beyond the SM can modify the top pair ($t\bar{t}$) production rate, therefore a measurement of the $t\bar{t}$ inclusive production cross section may reveal the presence of new physics. It can also help to verify the state-of-the-art theoretical cross section calculations, and to better understand $t\bar{t}$ production as one of the primary backgrounds in many searches for physics beyond the SM.

The inclusive top quark pair production cross section has been previously measured using different decay channels by the ATLAS experiment in pp collisions at 7 TeV [9–13]. All measurements have been found to be in good agreement with theoretical predictions for these energies. ATLAS has performed a measurement of the $t\bar{t}$ production cross section in the single-lepton channel at $\sqrt{s} = 8$ TeV using data corresponding to an integrated luminosity of $5.8\,\mathrm{fb}^{-1}$ [14]. The analysis is based on final states where one of the W bosons from the top decay decays leptonically into an electron or muon together with the corresponding neutrino, and the other decays hadronically. In this case the final state is characterized by the presence of a highly energetic and well isolated lepton, large missing transverse energy carried away by a neutrino, and at least four jets, two of which originate from b-quarks. A multivariate likelihood method is used to provide signal-to-background discrimination based on the lepton pseudorapidity and event aplanarity [15]. The likelihood discriminant distribution in data fitted to the sum of the signal and background templates is shown in Fig. 2 for both the electron and muon channel. The cross section is found to be

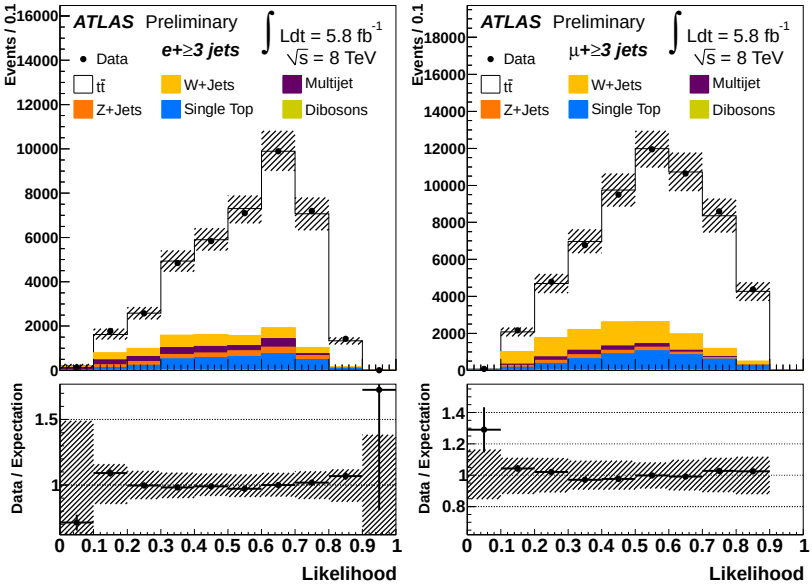

Figure 2: Fit to the likelihood discriminant $D(\eta_l, A')$ in data in the e+jets (left) and μ+jets (right) channels in $t\bar{t}$ production [14]. The hatched bands show the combined expected statistical and systematic uncertainty.

$\sigma_{t\bar{t}} = 241 \pm 2\ (\text{stat}) \pm 31\ (\text{syst}) \pm 9\ (\text{lumi})\,\text{pb}$. This result is in good agreement with the current theoretical prediction $\sigma_{t\bar{t}}^{\text{theor.}} = 238^{+22}_{-24}\,\text{pb}$ for a top quark mass of 172.5 GeV as obtained from approximate NNLO QCD calculations with HATHOR 1.2 [16]. Figure 3 shows the summary of all top pair production cross sections measured by ATLAS and the Tevatron as a function of the center of mass energy. Good agreement can be seen between the data and an the approximate NNLO QCD calculation based on HATHOR.

3.2 ZZ production

ATLAS has recently updated its measurement of the 7 TeV ZZ cross-section [17] with data taken at 8 TeV [18] corresponding to an integrated luminosity of $5.8\,\text{fb}^{-1}$. Candidate ZZ events are reconstructed in the $Z \to \ell^+\ell^-\ell^+\ell^-$ decay channel, where ℓ can be an electron or a muon. The electron and muon candidates are required to be isolated, have transverse momentum $p_{\text{T}} > 15$ GeV and $|\eta| < 2.5$. Same-flavour, oppositely-charged lepton pairs are combined to form Z candidates. A signal event must contain two such pairs with an invariant mass satisfying $66 < m_{\ell^+\ell^-} < 116$ GeV. This selection results in 85 observed ZZ candidate events whose invariant mass distribution is shown in Fig. 4 (left). The data-driven background expectation is 1.3 ± 1.3 events mostly due to events with a W/Z-boson decaying to leptons plus additional jets and photons, which are misidentified as electrons. The measured value of the total ZZ cross section is $\sigma_{ZZ}^{\text{tot}} = 9.3^{+1.1}_{-1.0}(\text{stat})^{+0.4}_{-0.3}(\text{syst}) \pm 0.3(\text{lumi})$ pb. This result is consistent with the SM prediction of $7.4 \pm 0.4\,\text{pb}$, calculated at NLO using MCFM and PDF set CT10. Figure 4 (right) shows this measurement together with the previous ZZ cross section measurements by ATLAS and the Tevatron experiments, as well as the theoretical predictions.

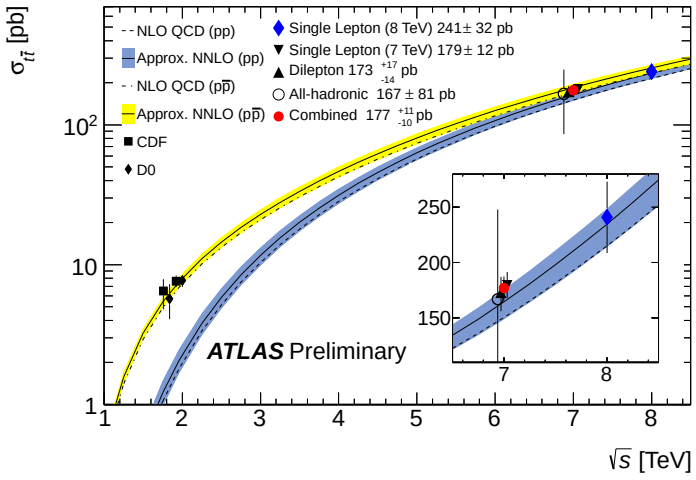

Figure 3: Top pair production cross section as a function of the center of mass energy [8]. The experimental results in the various top decay channels (and their combination) at 7 TeV and the recent result at 8 TeV are compared to an approximate NNLO QCD calculation based on HATHOR 1.2.

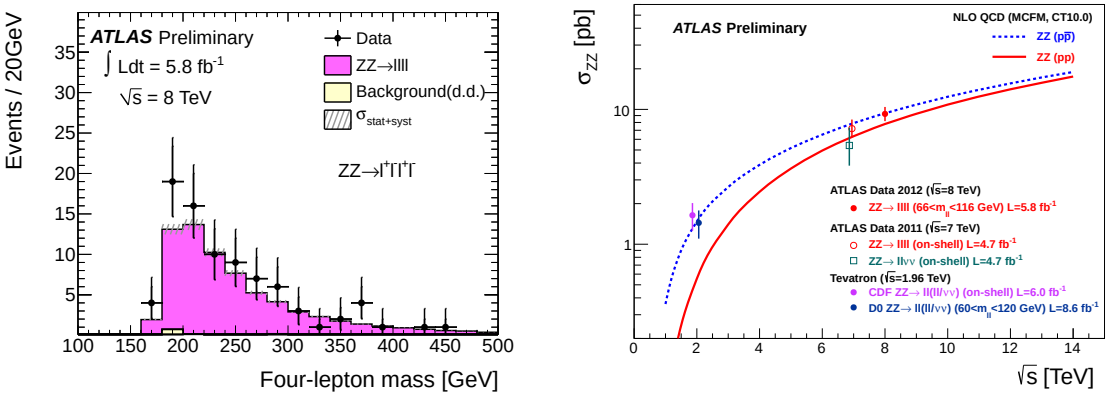

Figure 4: (left) Invariant mass of the four-lepton system for ZZ candidates [18]. The points are data and the stacked histograms show the signal and background predictions from simulation. The grey band indicates the combined statistical and systematic uncertainty on the signal prediction. (right) Measurements and theoretical predictions of the total ZZ production cross section as a function of centre-of-mass energy. The blue dashed line shows the theoretical prediction for the ZZ production cross section in proton anti-proton collisions, calculated at NLO in QCD using MCFM with PDF set CT10. The solid red line shows the theoretical prediction for the ZZ production cross section in proton proton collisions, calculated in the same way.

4. Searches for the Standard Model Higgs boson

During the summer of 2012 both the ATLAS and CMS collaborations have reported the observation of a Higgs-like particle with a mass of approximately 125 GeV [19, 20]. Since then ATLAS has updated its main analyses with up to $13\,\text{fb}^{-1}$ of data collected at $\sqrt{s} = 8$ TeV and the results are reported in the following for the channels $H \to \tau\tau$, $H \to b\bar{b}$, $H \to WW$, $H \to \gamma\gamma$ and $H \to 4\ell$. In addition, the combination of all channels and an analysis of the spin and parity using the four-lepton channel is shown.

4.1 Search for $H \to \tau\tau$ and $H \to b\bar{b}$

Using $4.6\,\text{fb}^{-1}$ of data collected at $\sqrt{s} = 7$ TeV and $13.0\,\text{fb}^{-1}$ of data collected at $\sqrt{s} = 8$ TeV ATLAS has performed a search [21] for the SM Higgs boson decaying to two τ leptons where the τ lepton is decaying either leptonically or hadronically resulting in three different final state topologies ($\tau_{\text{lep}}\tau_{\text{lep}}$, $\tau_{\text{lep}}\tau_{\text{had}}$ and $\tau_{\text{had}}\tau_{\text{had}}$). The selected event samples are split into 25 exclusive categories according to the number and kinematic properties of reconstructed jets. The invariant mass is the final discriminating observable used for all categories. No significant excess is observed in the data compared to the SM background-only expectation in any of the channels. Figure 5 (left) shows the observed (expected) upper limit at 95% CL on the cross-section times branching ratio for SM $H \to \tau\tau$ and is found to be 1.9 (1.2) times the SM prediction for a Higgs boson with mass $m_H = 125$ GeV. For this mass, the observed (expected) deviation from the background-only hypothesis corresponds to a local significance of 1.1 (1.7) standard deviations and the best fit value of $\mu = 0.7 \pm 0.7$.

At a mass of 125 GeV the SM Higgs boson is expected to predominately decay into a pair of b quarks. Due to the overwhelming QCD background the search is carried out in the associate production mode with a W or Z boson and using the lepton from the associated vector boson to significantly reduce the backgrounds. This results in the following final states: $ZH \to \nu\bar{\nu}b\bar{b}$, $WH \to \ell\nu b\bar{b}$ and $ZH \to \ell^+\ell^- b\bar{b}$. The analysis [22] has been carried out in 16 different categories depending on the number of leptons, number of jets and the transverse momentum of the vector boson candidate. No significant excess is observed. For $m_H = 125$ GeV, the observed (expected) upper limit on the production cross section times the branching ratio is found to be 1.8 (1.9) times the SM prediction and can be seen in Fig. 5 (right).

4.2 Search for $H \to WW$

The $H \to WW^{(*)} \to \ell\nu\ell\nu$ channel (with $\ell = e, \mu$) provides important information on both the overall production rate and the coupling to W bosons. ATLAS has performed a search using $13.0\,\text{fb}^{-1}$ of data collected at $\sqrt{s} = 8$ TeV and using the most sensitive final state $e\nu\mu\nu$ [23]. A transverse mass variable (m_{T}) is used to test for the presence of a signal and the resulting distribution for data and background is shown in Fig. 6 (left). An excess of events over the expected background is observed for $m_H < 150$ GeV, with a significance of 2.8 standard deviations as seen on the right of Fig. 6. The best fit signal strength at $m_H = 125$ GeV is $\mu = 1.5 \pm 0.6$, which translates into a measured cross section times branching ratio of $\sigma(pp \to H) \times \text{BR}(H \to WW) = 7.0^{+1.7}_{-1.6}(\text{stat})^{+1.7}_{-1.6}(\text{syst theor}) \pm 1.3(\text{syst exp}) \pm 0.3(\text{lumi})\,\text{pb}$.

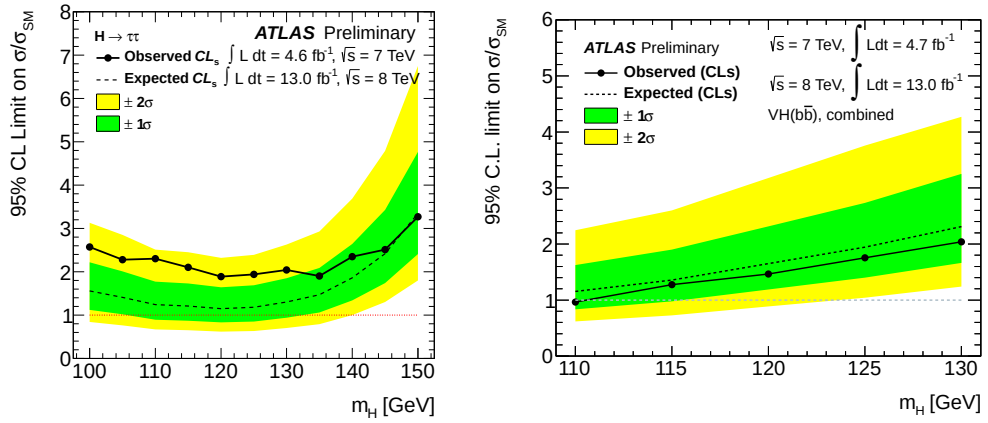

Figure 5: Observed (solid) and expected (dashed) 95% confidence level upper limits on the Higgs boson cross-section times branching ratio, normalised to the SM expectation, as a function of the Higgs boson mass for $H \to \tau\tau$ (left) [21] and $H \to b\bar{b}$ (right) [22]. Expected limits are given for the scenario with no signal. The bands around the dashed line indicate the $\pm 1\sigma$ and $\pm 2\sigma$ uncertainties of the expected limit.

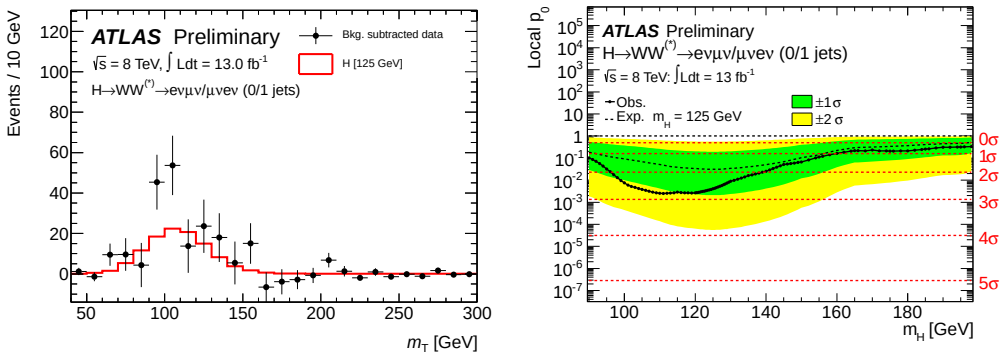

Figure 6: (left) The m_{T} distribution in data with the estimated background subtracted, overlaid with the predicted signal for $m_H = 125$ GeV for the combined 0/1-jet data set in the $H \to WW$ channel [23]. (right) Observed (solid line) probability for the background-only scenario, p_0, as a function of m_H. The dashed line shows the corresponding expectation for the $m_H = 125$ GeV hypothesis.

4.3 Search for H $\to \gamma\gamma$

The results of the previous ATLAS Higgs boson searches in the diphoton decay channel [19] were obtained with a combination of $4.8\,\mathrm{fb}^{-1}$ of data recorded at $\sqrt{s} = 7$ TeV and $5.9\,\mathrm{fb}^{-1}$ of data recorded at $\sqrt{s} = 8$ TeV and showed an excess of events with a diphoton invariant mass compatible with a SM Higgs boson mass of 126.5 GeV. ATLAS has updated this measurement [24] with an enlarged dataset of $13.0\,\mathrm{fb}^{-1}$ recorded at $\sqrt{s} = 8$ TeV between July and September 2012 and combined the result with the previous $\sqrt{s} = 7$ TeV results, which are unchanged from the previous publication [25]. In the final offline event selection at least two photons satisfying tight identification criteria based on the shapes of the electro-magnetic showers and transverse energies for the leading and sub-leading photons are required to be larger than 40 GeV and 30 GeV, respectively. In addition to the identification criteria, both photons are also required to be isolated through the

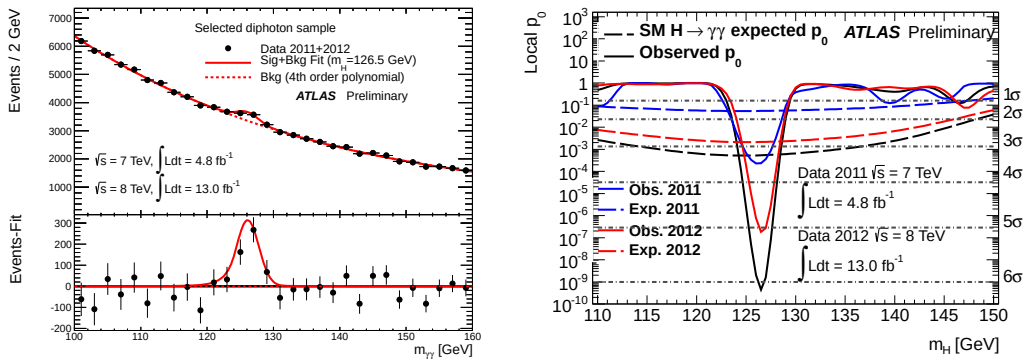

Figure 7: (left) Invariant mass distribution of diphoton candidates in the $H \to \gamma\gamma$ channel [24] for the combined 7 and 8 TeV data samples. The result of a fit to the data of the sum of a signal component fixed to $m_H = 126.5$ GeV and a background component described by a fourth-order Bernstein polynomial is superimposed. (right) The observed local p-value as a function of m_H. The corresponding expected local p_0 values for the SM Higgs boson signal plus background hypothesis are shown by the dashed curves.

use of criteria based on both the inner tracker and the calorimeter. The events are classified into 10(12) categories for the 7(8) TeV dataset based on the rapidity and p_{T} of the photon candidates, whether they are converted photons or not and the number of jets and leptons in the event. The categories differ in signal-to-background ratio as well as invariant mass resolution and thus increase the sensitivity of the search. The inclusive diphoton invariant mass distribution for the combined $\sqrt{s} = 7$ TeV and $\sqrt{s} = 8$ TeV data samples is shown in Fig. 7 (left) including an overlaid signal-plus-background fit and a background subtracted diphoton mass spectrum. An excess of events around $m_H = 126.5$ GeV is observed with a best-fit mass of $m_H = 126.6 \pm 0.3(\mathrm{stat}) \pm 0.7(\mathrm{syst})$ GeV and a signal strength of $\mu = 1.80 \pm 0.30(\mathrm{stat})^{+0.21}_{-0.15}(\mathrm{syst})^{+0.20}_{-0.14}(\mathrm{theor})$, which is 2.4 standard deviations from the SM expectation. The local significance of the excess is 6.1σ as shown in Fig. 7 (right). Taking into account the look-elsewhere effect, the global significance of the excess is 5.4σ.

4.4 Search for H $\to 4\ell$

Using the same data sample as in the previous section, ATLAS has performed an updated measurement of the SM Higgs boson decaying into four leptons [26] via the the decay $H \to ZZ^{(*)} \to 4\ell$, where $\ell = e, \mu$ resulting in the four distinct final states 4μ, $2\mu 2e$, $2e2\mu$ and $4e$. For the mixed lepton pair final states, the first lepton pair is the ones closest to the Z-pole mass. Each electron (muon) must satisfy $E_T > 7$ GeV ($p_{\mathrm{T}} > 6$ GeV) and the three highest p_{T} leptons must satisfy $p_{\mathrm{T}} > 20, 15, 10$ GeV, respectively. The leptons are required to be separated from each other by $\Delta R > 0.1$ if they are of the same flavour and $\Delta R > 0.2$ otherwise. The combined signal reconstruction and selection efficiency for $m_H = 125$ GeV is 37% for the 4μ channel, 23% for the $2e2\mu/2\mu 2e$ channel and 20% for the $4e$ channel. Figure 8 (left) shows the four-lepton invariant mass distribution for the combined dataset and the expectation for a 125 GeV SM Higgs boson. An excess of events is observed with a best-fit mass of $m_H = 123.5 \pm 0.9(\mathrm{stat}) \pm 0.3(\mathrm{syst})$ GeV and a signal strength of $\mu = 1.3^{+0.5}_{-0.4}$ times the SM model expectation. The local significance of the excess is 4.1σ as can be seen on the right of Fig. 8.

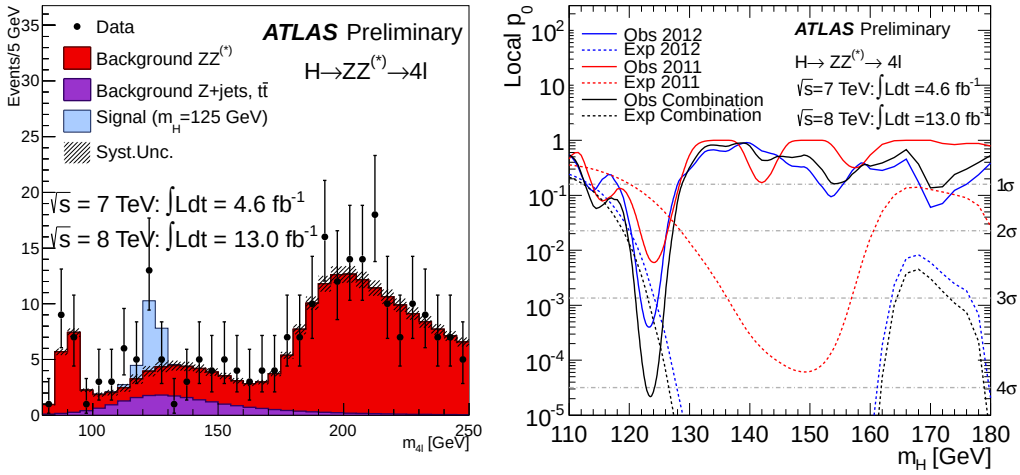

Figure 8: (left) The distribution of the four-lepton invariant mass in $H \to 4\ell$ [26], $m_{4\ell}$, for the selected candidates compared to the background expectation for the combined data sets together with the signal expectation for a $m_H = 125$ GeV Higgs boson. (right) The observed local p-value for the combination of the 2011 and 2012 data sets (solid lines). The dashed curves show the expected median local p-value for the signal hypothesis when tested at the corresponding m_H.

4.5 Combination of Higgs measurements

Figure 9 (left) shows a summary of the measured signal strength parameter for the individual Higgs decay channels and their combination giving an average value of $1.35 \pm 0.19\,(\text{stat}) \pm 0.15\,(\text{syst})$ computed at the mass of 125 GeV [27]. A compatibility test between the observed signal strengths of the five channels and the SM expectation of unity gives a probability of about 13%. The mass measurement, based on fits to the spectra of the high mass resolution channels $H \to \gamma\gamma$ and $H \to ZZ \to 4\ell$, is $m_H = 125.2 \pm 0.3\,(\text{stat}) \pm 0.6\,(\text{sys})$ GeV and can be seen in Fig. 9 (right). The difference of the mass measurements between these two channels is $3.0 \pm 0.8\,(\text{stat})\,^{+0.7}_{-0.6}\,(\text{sys})$ GeV, corresponding to about 2.7 standard deviations, using Gaussian error distributions for systematic uncertainties. A more conservative treatment of the systematic uncertainty related to the mass scale, using rectangular error distributions for parts of the uncertainties, reduces the difference to the level of 2.3 standard deviations. In summary, the measured properties of the new boson are consistent with the expectations of the SM Higgs boson.

4.6 Spin and parity analysis in the four-lepton channel

For $H \to ZZ^{(*)} \to 4\ell$ decays, the observables sensitive to the underlying spin and parity of H are the masses of the two Z bosons, the production angle and the four decay angles. Using this information ATLAS has performed a study testing the four spin and parity hypotheses $J^P = 0^+, 0^-, 2^+$ and 2^- [26]. A boosted decisions tree (BDT) is used to form a J^P discriminant for each pair of spin/parity states using the expected distributions for the production and decay angles. Figure 10 (left) shows the BDT discriminant for data and Monte Carlo for the 0^+ and 0^- hypotheses and the right plot shows the resulting log-likelihood ratio. The same procedure is carried out for all pairs of spin/parity combinations. The SM spin and parity remains the favoured hypothesis, with the other

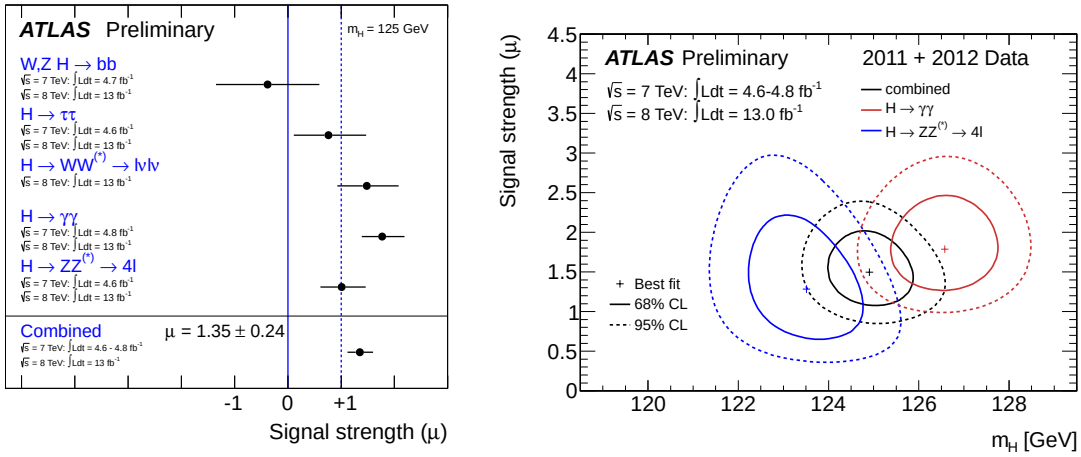

Figure 9: (left) Measurements of the signal strength parameter μ for $m_H = 125$ GeV for the individual channels and for their combination [27]. (right) Confidence intervals in the (μ, m_H) plane for the $H \to ZZ^{(*)}$ and $H \to \gamma\gamma$ channels and their combination, including all systematic uncertainties. The markers indicate the maximum likelihood estimates (μ, m_H) in the corresponding channels.

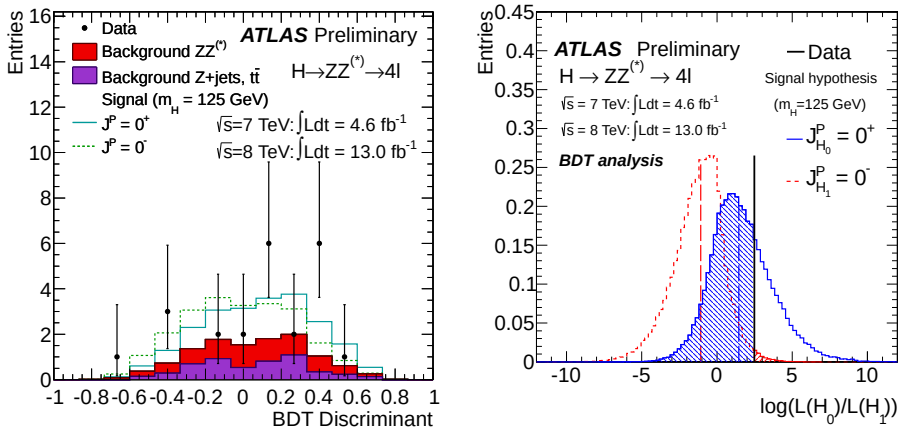

Figure 10: (left) Distribution of the BDT discriminant for data and Monte Carlo expectations for the 0^+ and 0^- hypotheses. (right) Distributions of the log-likelihood ratio generated with more than 50,000 Monte Carlo pseudo-experiments when assuming the spin 0^+ hypothesis and testing the 0^-. The data are indicated by the solid vertical line, and the median of the expected distribution is indicated by a dashed line. The shaded areas correspond to the observed p_0-values, representing the compatibility with the tested hypothesis 0^- (right shaded area) and the assumed hypothesis 0^+ (left shaded area) [26].

spin parity hypotheses excluded at the following level: 98.9% for 0^-, 84% for 2^+ and 97.1% for 2^-. The same analysis is carried out using a matrix element based likelihood ratio (MELA) instead of the BDT with very similar results.

5. Searches for Supersymmetry

ATLAS has executed in the last years an extensive Supersymmetry (SUSY) search program without any significant deviations from the SM observed so far. The inclusive SUSY searches, i.e.

searches for events with an excess of missing energy with zero [28] or one lepton [29] in the final state, indicate that the masses of gluinos and first/second generation squarks are expected to be above 1 TeV. However in order to solve the hierarchy problem in a "natural" way, the masses of the superpartners of the top, bottom and gauge bosons need to be below the TeV-scale to properly cancel the divergences in the Higgs mass radiative corrections. Despite their production cross sections being smaller than for the first and second generation squarks, stop and sbottom may well be directly produced at the LHC and could provide the only direct observation of SUSY at the LHC in case the other sparticles are outside of the LHC energy reach. The lightest mass eigenstates of the sbottom and stop particles, $\tilde{b}_1$ and $\tilde{t}_1$, could hence be produced either directly in pairs or through $\tilde{g}$ pair production followed by $\tilde{g} \to \tilde{b}_1 b$ or $\tilde{g} \to \tilde{t}_1 t$ decays.

5.1 Search for direct sbottom pair production

ATLAS has performed a search for direct sbottom pair production using $12.8\,\text{fb}^{-1}$ collected in 2012 at a centre-of-mass energy of 8 TeV [30]. The analysis uses three different signal regions for optimal sensitivity to the kinematic topologies associated to different mass-splittings between the sbottom and neutralino mass. Signal events are are selected based on the missing transverse momentum $E_{\text{T}}^{\text{miss}}$ and boost-corrected contransverse mass m_{CT} [31], two high-p_{T} b-tagged leading jets and no electron or muons. The dominant background processes in the signal regions are top and W plus heavy flavour production. All backgrounds are estimated using a combination of Monte Carlo and data-driven techniques. Figure 11 (left) shows the $E_{\text{T}}^{\text{miss}}$ distribution in one of the signal regions together with the expectations from the various background sources and a SUSY sample with the relevant mass difference between sbottom and neutralino. No excess above the SM expectations is observed in any of the signal regions. In addition to obtaining model-independent upper limits on the number of expected beyond the SM signal events, these results are also interpreted in a specific SUSY scenario, which assumes a sparticle mass hierarchy such that the sbottom decays exclusively via $\tilde{b}_1 \to b\tilde{\chi}_1^0$. Figure 11 (right) shows the exclusion limit obtained by taking in each point the signal region with the best expected exclusion. The results are in agreement with SM predictions for backgrounds and translate into 95% confidence level (CL) upper limits on sbottom and neutralino masses for the given MSSM scenario. Sbottom masses up to 620 GeV are excluded for $m_{\tilde{\chi}_1^0} = 0$. Differences in mass above 40 GeV between the $\tilde{b}_1$ and $\tilde{\chi}_1^0$ are excluded up to sbottom masses of 300 GeV. Neutralino masses up to 320 GeV are excluded for sbottom masses around 550 GeV.

5.2 Direct searches for stop production

Depending on the mass of the stop, two decay channels can be distinguished: $\tilde{t} \to t\tilde{\chi}_1^0$ and $\tilde{t} \to b\tilde{\chi}_1^+ \to bW^+\tilde{\chi}_1^0$. ATLAS has a wide range of different analysis in each of these modes at both 7 TeV and 8 TeV centre-of-mass energy. Reference [32] reports on the search for stop quarks in final states with two leptons using $13\,\text{fb}^{-1}$ collected at 8 TeV in the decay channel $\tilde{t} \to b\tilde{\chi}_1^+ \to bW^+\tilde{\chi}_1^0$. The analysis selects events with two b quarks, two W bosons and additional $E_{\text{T}}^{\text{miss}}$ resulting mainly from the undetected $\tilde{\chi}_1^0$. The number of observed events has been found to be consistent with the SM expectation. Limits have been set on the mass of a supersymmetric scalar top for different assumptions on the mass hierarchy scalar top-chargino-lightest neutralino. A scalar top quark of mass between 150 and 450 GeV is excluded at 95% CL for a massless neutralino and a chargino

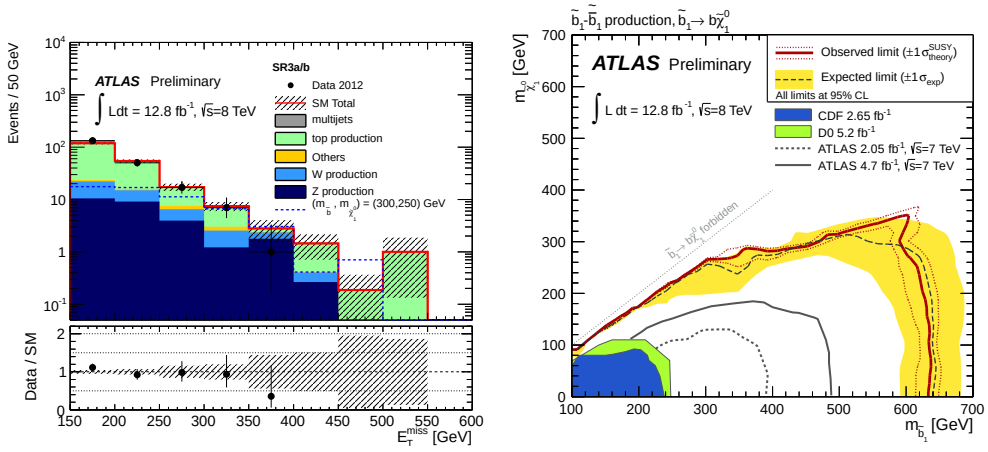

Figure 11: (left) $E_{\mathrm{T}}^{\mathrm{miss}}$distribution in one of the signal regions (assuming p_{T} of the leading jet larger than 130 GeV) in the search for direct sbottom pair production [30]. The shaded band includes both detector and theoretical systematic uncertainties. The backgrounds are normalised to the values determined in the fit. (right) Expected and observed exclusion limits at 95% CL in the $(m_{\tilde{b}_1}, m_{\tilde{\chi}_1^0})$ plane obtained taking in each point the signal region which gives the best expected CL exclusion. The black, dashed line shows the expected limit if theory uncertainties on the signal are neglected. The yellow band shows the $\pm 1\sigma$ Gaussian equivalent uncertainty on the expected limit. The red solid line shows the nominal observed limit, while the red dashed lines show its variation if theory uncertainties on the signal are taken into account.

approximately degenerate with the scalar top quark. For a massless neutralino and a 200 GeV chargino the 95% CL exclusion range on the scalar top quark mass is $200-335$ GeV. For a 300 GeV scalar top quark and a 290 GeV chargino, models with a neutralino with mass lower than 175 GeV are excluded at 95% CL. Figure 12 shows the exclusion limits on the neutralino and stop masses for a fixed value of $m_{\tilde{t}} - m_{\tilde{\chi}_1^{\pm}} = 10$ GeV.

For the case of a high-mass stop decaying to a top and neutralino ($\tilde{t} \to t\tilde{\chi}_1^0$) an analysis for direct stop pair production in final states with one isolated lepton, jets and missing transverse momentum has been done [33]. Three different signal regions are defined based on three different benchmark models for specific $m(\tilde{t}_1, \tilde{\chi}_1^0)$ mass points. All signal regions require a selection on the 3-jet mass of the hadronically decaying top quark to reject the $t\bar{t}$ background where both W bosons from the top quarks decay leptonically. For increasing stop mass and increasing mass difference between the stop and neutralino, the requirements on $E_{\mathrm{T}}^{\mathrm{miss}}$ and other selection variables are tightened. No significant excess of events above the rate predicted by the SM is observed and 95% CL upper limits are set on the stop mass in the stop-neutralino mass plane. The region of excluded stop and neutralino masses is shown on the right in Fig. 12. Stop masses are excluded between 225 GeV and 560 GeV for massless neutralinos, and stop masses around 500 GeV are excluded along a line which approximately corresponds to neutralino masses up to 175 GeV.

6. Heavy ion physics

During 2010 and 2011 ATLAS recorded lead-lead (Pb+Pb) collision events corresponding to an integrated luminosity of $160\,\mu b^{-1}$ at a (per-nucleon) centre-of-mass energy of $\sqrt{s_{NN}} =$

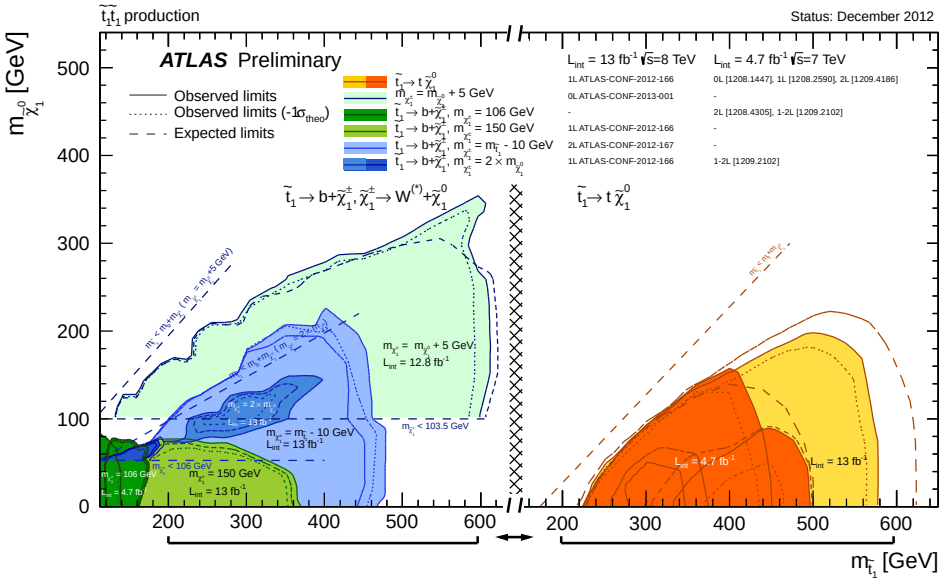

Figure 12: Summary [8] of the dedicated searches for stop pair production based on 13 fb^{-1} of pp collision data taken at $\sqrt{s} = 8$ TeV [32–34] and 4.7 fb^{-1} of data taken at $\sqrt{s} = 7$ TeV [35–39]. Exclusion limits at 95% CL are shown in the $\tilde{\chi}_1^0$-$\tilde{t}_1$mass plane for the decay modes $\tilde{t} \to b\tilde{\chi}_1^{\pm} \to bW^{\pm}\tilde{\chi}_1^0$ (left) and $\tilde{t} \to t\tilde{\chi}_1^0$ (right). The dashed and solid lines show the expected and observed limits, respectively, including all uncertainties except the theoretical signal cross section uncertainty (PDF and scale). The dotted lines represent the results obtained when reducing the nominal signal cross section by 1σ of its theoretical uncertainty.

2.76 TeV. In addition, proton-lead collisions at $\sqrt{s_{NN}} = 5.02$ TeV were recorded during a short pilot run in September 2012 when the LHC collided a 4 TeV proton beam with a 1.57 TeV per-nucleon Pb beam resulting in approximately 1 μb^{-1} of integrated luminosity.

The geometry of a heavy ion (HI) collision is typically described via the centrality, which reflects the overlap volume of the two colliding nuclei. Collisions with a small (large) impact parameter are referred to as central (peripheral). The overlap volume is closely related to the average number of participant nucleons which scatter inelastically in each nuclear collision, $\langle N_{\text{part}} \rangle$, and to the average number of binary collisions between the nucleons of the colliding nuclei, $\langle N_{\text{coll}} \rangle$. In ATLAS centrality is measured using the scalar sum of transverse energy ($\sum E_T$) deposited in the FCal. Events are divided into centrality classes expressed in percentiles of the total inelastic non-Coulomb lead-lead cross-section with the most central interval (0-10%) corresponding to the 10% of events with the largest FCal energy deposit.

6.1 Z bosons in Pb+Pb Collisions

The hot and dense matter produced in HI collisions causes a significant energy loss of energetic colour-charge carries when propagating through that medium. An understanding of this phenomenon requires measuring the unmodified production rates of the particles before they lose energy. The best candidates to perform such measurements are particles that do not interact via the strong force, e.g. Z bosons decaying into electrons or muons. Using an integrated luminosity of 0.15 nb^{-1} collected during the 2011 Pb+Pb LHC run, ATLAS has performed a measurement of the Z boson production at $\sqrt{s_{NN}} = 2.76$ TeV [40]. Z boson candidates are reconstructed in the

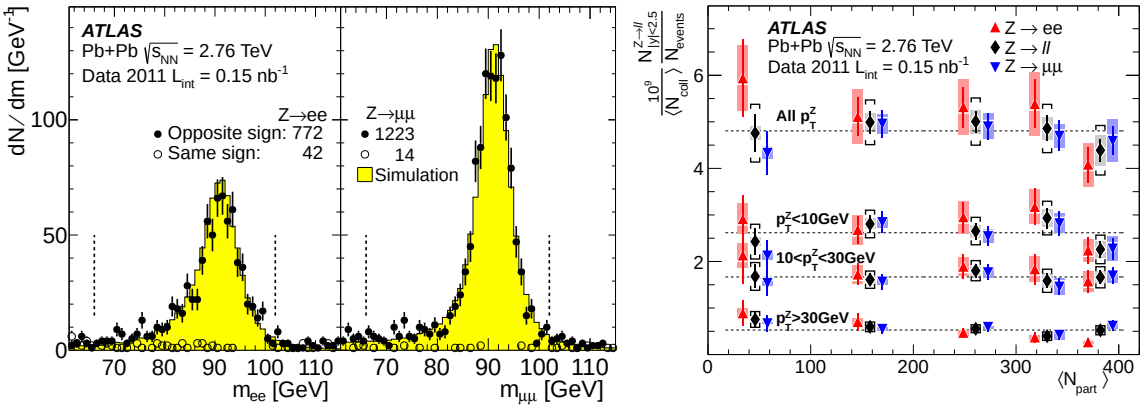

Figure 13: (left) The invariant mass distributions of $Z \to ee$ and $Z \to \mu\mu$ candidates [40] with statistical uncertainties. The number of opposite and same sign lepton pairs is listed for the region $66 < m_{\ell\ell} < 102$ GeV. The Monte Carlo is weighted to match the centrality distribution in data and normalised in the same region. (right) Centrality dependence of Z boson yields divided by $\langle N_{\rm coll} \rangle$. Results for ee (upward pointing triangles) and $\mu\mu$ (downward pointing triangles) channels are shifted left and right, respectively, from their weighted average (diamonds) for display purposes. Bars and boxes represent statistical and systematic uncertainties, respectively. For the combined results, the brackets show the combined uncertainty including the uncertainty on $\langle N_{\rm coll} \rangle$, and the dashed line is a fit using a constant.

di-electron and di-muon channel using special reconstruction algorithms adapted to the HI environment. The background contribution is estimated via same-sign lepton pairs in the signal region defined as $66 < m_{\ell\ell} < 102$ GeV ($\ell = e, \mu$). The $m_{\ell\ell}$ invariant mass distributions for both signal and combinatorial background events are shown in Fig. 13 (left). In total 772 (1223) opposite-sign $Z \to ee$ ($Z \to \mu\mu$) candidates are reconstructed with a very small background of 42 (14) same-sign pairs. To examine the binary collision scaling of the data, the Z boson per-event yields, divided by $\langle N_{\rm coll} \rangle$, are shown in Fig. 13 (right) as a function of $\langle N_{\rm part} \rangle$, in several $p_{\rm T}^Z$ bins. The figure demonstrates that the $Z \to ee$ and $Z \to \mu\mu$ results are consistent within their uncertainties for all $p_{\rm T}^Z$ and centrality regions. Within the statistical significance of the data sample, the Z boson per-event yield obeys binary collision scaling.

Building on this analysis, ATLAS has performed a measurement of the jet quenching effects (momentum imbalance) in $Z \to \ell\ell$+jet events using the same data sample [41]. Each event containing a Z boson candidate was scanned for jets reconstructed with an anti-k_t algorithm [42] using three different cone sizes of 0.2, 0.3 and 0.4. In the HI environment there is a significant energy deposition in the calorimeters due to the underlying event that must be removed in order to accurately reconstruct jets. At the same time it has to be taken care that the energy of the jet is not included in the background estimation for the underlying event. Details of HI jet reconstruction are discussed in Ref. [43]. Jets were required to have a minimum $p_{\rm T}$ of 25 GeV and only the jet with the highest transverse momentum in an event was considered for the Z+jet candidates. To choose Z bosons and jets that are correlated with each other, and likely originate in the same initial hard scattering, only pairs that are separated by at least $\pi/2$ in azimuthal angle were considered. After all selections 36 $Z \to \ell\ell$+jet candidates were reconstructed. Figure 14 shows the means of the $p_{\rm T}^{\rm jet}/p_{\rm T}^Z$ distributions for the different centrality bins and jet cone sizes. It clearly shows a suppression compared to the

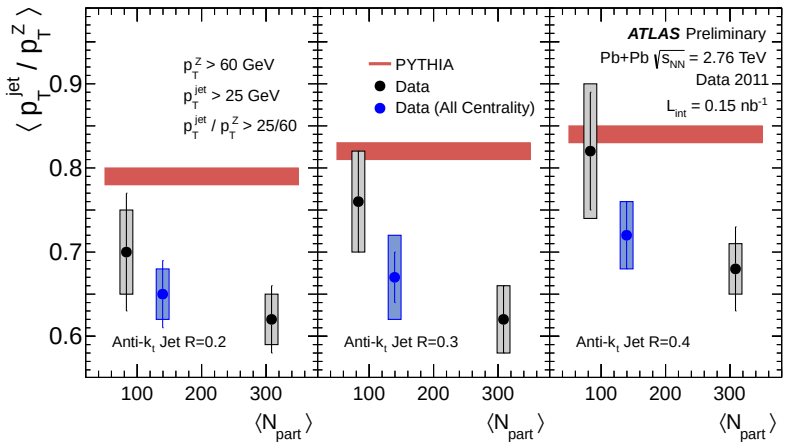

Figure 14: The extracted means from the $p_{\mathrm{T}}^{\mathrm{jet}}/p_{\mathrm{T}}^{Z}$ distributions of the fully corrected data plotted as a function of $\langle N_{\mathrm{coll}} \rangle$, for each of the three considered jet cone sizes [41]. The data are compared to a baseline of PYTHIA, which does not contain any jet energy loss mechanisms. Bars represent statistical uncertainties, and shaded boxes systematic uncertainties. The systematic uncertainties are largely correlated across the $\langle N_{\mathrm{coll}} \rangle$bins. The width of the PYTHIA band represents its uncertainty. The blue points refer to 0-80% centrality, and therefore are not independent relative to the black points.

PYTHIA generated events, which contains no energy loss mechanism and thereby serves as a baseline for judging jet quenching effects. These results are qualitatively consistent with the expectation of energy loss in jets as they traverse the hot dense medium created in HI collisions.

6.2 Heavy flavour production

High-p_{T} quarks and gluons generated in hard scattering processes during the initial stages of the heavy collisions are thought to lose energy in the quark-gluon plasma resulting in "jet quenching". Since the energy loss results from the interaction of a quark or a gluon with the medium, jet quenching is thought to provide a valuable tool for probing the properties of the quark-gluon plasma. ATLAS has performed a measurement of inclusive muon production in Pb+Pb collisions at $\sqrt{s_{NN}} = 2.76$ TeV using an integrated luminosity of approximately $7\mu b^{-1}$ collected in 2010 [44]. The measurements were performed for several intervals of collision centrality over the muon transverse momentum range $4 < p_{\mathrm{T}} < 14$ GeV and the yields compared to those in a peripheral bin using the "central-to-peripheral" ratio $R_{CP} \equiv \langle N_{\mathrm{coll}} \rangle^{\mathrm{periph}} \mathrm{d}n^{\mathrm{cent}} / \langle N_{\mathrm{coll}} \rangle^{\mathrm{cent}} \mathrm{d}n^{\mathrm{periph}}$ where $\mathrm{d}n^{\mathrm{cent}}$ and $\mathrm{d}n^{\mathrm{periph}}$ represent the per-event differential rate for the same hard-scattering observable in central and peripheral collisions, respectively. In this p_{T} range, muon production in pp collisions results predominantly from semi-leptonic decays of charm and bottom quarks. All other sources including J/ψ decays contribute less than 1% of the prompt muon yield. To separate signal from background muons a discriminant C is used that combines the information from momentum loss in the calorimeter and the deflection in the inner detector and is described in detail in Ref. [44]. Figure 15 (left) shows the C-distribution for signal and background muons derived from Monte Carlo samples. From these distributions templates are extracted that are used to extract the fraction of signal muons on the data. The resulting value of R_{CP} for different p_{T} ranges and centrality intervals is shown on the right side of Fig. 15. This indicates a factor of about 2.5 suppression in the yield of

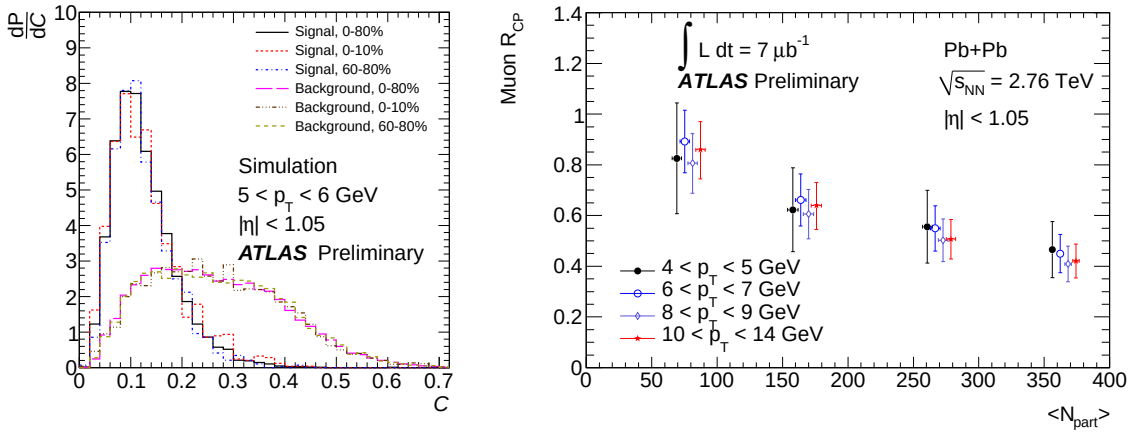

Figure 15: Analysis of inclusive muon production in Pb+Pb collisions at $\sqrt{s_{NN}} = 2.76$ TeV [44]. (left) Simulated distributions of the muon discriminant C for signal and background muons for different centrality classes for muons in the momentum range $5 < p_{\mathrm{T}} < 6$ GeV. (right) Muon R_{CP} as a function of $\langle N_{\mathrm{part}} \rangle$ for different bins in muon p_{T}. The error bars show combined statistical and systematic uncertainties. The sets of points for the different p_{T} bins are successively displaced by Delta $\langle N_{\mathrm{part}} \rangle = 6$ for clarity of presentation.

muons in the most central (0-10%) collisions compared to the most peripheral collisions included in the analysis (60-80%). The central R_{CP} is $1.5-2$ times larger than that measured for charged hadrons in a comparable p_{T} range and using comparable, though not identical, centrality ranges. The central R_{CP} indicates weaker suppression than observed in the semi-leptonic electron channel measured over the same p_{T} range in $\sqrt{s_{NN}} = 200$ GeV Au+Au collisions at RHIC.

6.3 Two-particle correlations in proton-lead collisions

The first studies of two-particle correlation functions in the highest-multiplicity pp collisions at the LHC [45] showed an enhanced production of pairs of particles at $\Delta\phi \sim 0$, with the correlation extending over a wide range in $\Delta\eta$ (the "ridge"). To provide further insight into the physical origin of the these long-range correlations ATLAS has performed a measurement of the two-particle correlations $C(\Delta\phi, \Delta\eta)$ in relative azimuthal angle ($\Delta\phi$) and pseudorapity ($\Delta\eta$) using $1\mu b^{-1}$ of data collected in $\sqrt{s_{NN}} = 5.02$ TeV proton-lead collisions [46]. The correlation function is given by $C(\Delta\phi, \Delta\eta) = S(\Delta\phi, \Delta\eta)/B(\Delta\phi, \Delta\eta)$ where $\Delta\phi = \phi_a - \phi_b$ and $\Delta\eta = \eta_a - \eta_b$ represent pair distributions of two particles a and b constructed from the same event (S) and from "mixed events" (B), respectively. Figure 16 (a) and (b) show examples of 2-D correlation functions for charged particles with $0.5 < p_{\mathrm{T}} < 4$ GeV in peripheral and central events. The correlation function for peripheral events shows a sharp peak centered at $(\Delta\phi, \Delta\eta) = (0,0)$ due to pairs originating from the same jet, Bose-Einstein correlations, as well as high-p_{T} resonance decays, and a broad structure at $\Delta\phi \sim \pi$ from dijets, low-p_{T} resonances, and momentum conservation that is collectively referred to as "recoil". In the central events, the correlation function reveals a ridge-like structure at $\Delta\phi \sim 0$ (the "near-side") that extends over the full measured $\Delta\eta$ range, with an amplitude of a few percent. The distribution at $\Delta\phi \sim \pi$ (the "away-side") is also broadened relative to peripheral events, consistent with the presence of a long-range component in addition to that seen in peripheral events. To quantify the strength of these long-range correlations, it is convenient to define the "per-trigger yield,"

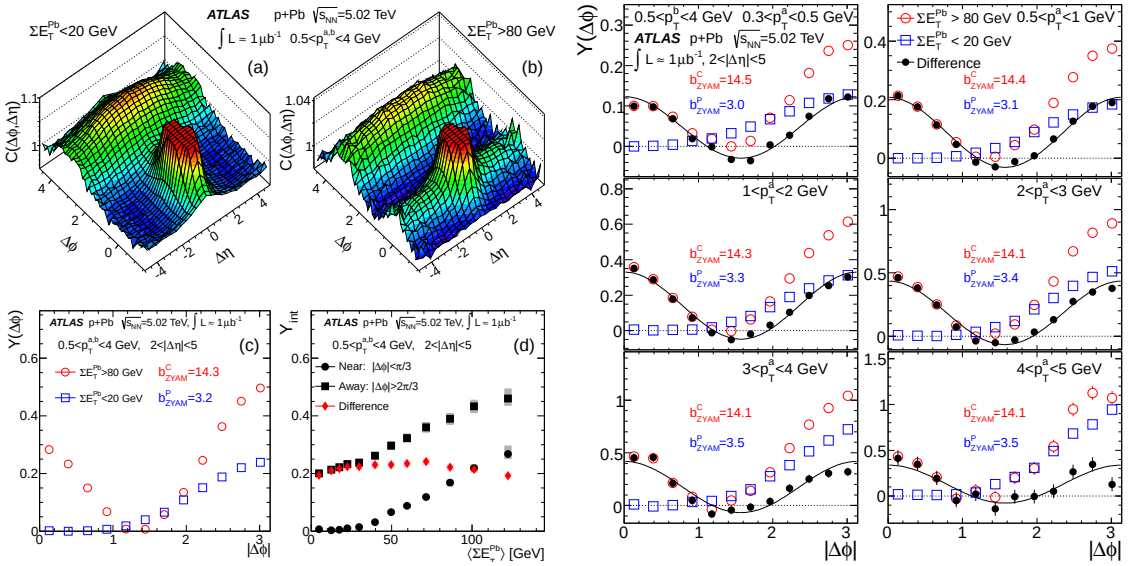

Figure 16: Two-particle correlations in proton-lead collisions [46]. (left) Two-dimensional correlation functions for (a) peripheral events and (b) central events, both with a truncated maximum to suppress the large correlation at $(\Delta\eta,\Delta\phi)=(0,0)$; (c) the per-trigger yield $\Delta\phi$ distribution together with pedestal levels for peripheral ($b^{\mathrm{P}}_{\mathrm{ZYAM}}$) and central ($b^{\mathrm{C}}_{\mathrm{ZYAM}}$) events, and (d) integrated per-trigger yield as function of $\sum E_{\mathrm{T}}^{\mathrm{Pb}}$ or pairs in $2<|\Delta\eta|<5$. The shaded boxes represent the systematic uncertainties, and the statistical uncertainties are smaller than the symbols. (right) Distributions of per-trigger yield in the peripheral and the central event activity classes and their differences (solid symbols), for different ranges of $p_{\mathrm{T}}^{\mathrm{a}}$ and $0.5<p_{\mathrm{T}}^{\mathrm{b}}<4$ GeV, together with functions $a_0+2a_2\cos(2\Delta\phi)$ obtained via a Fourier decomposition. The values for the ZYAM-determined pedestal levels are indicated on each panel for peripheral ($b^{\mathrm{P}}_{\mathrm{ZYAM}}$) and central ($b^{\mathrm{C}}_{\mathrm{ZYAM}}$) $\sum E_{\mathrm{T}}^{\mathrm{Pb}}$ bins.

$(Y(\Delta\phi))$ which measures the average number of particles correlated with each trigger particle:

$$Y(\Delta\phi)=\left(\frac{\int B(\Delta\phi)d\Delta\phi}{\pi N_a}\right)C(\Delta\phi)-b_{\mathrm{ZYAM}},$$

where N_a denotes the total number of trigger particles, $B(\Delta\phi)$ represents the pair distribution arising from uncorrelated pairs, and b_{ZYAM} their pedestal. Figure 16 (c) shows the $Y(\Delta\phi)$ distributions for $2<|\Delta\eta|<5$ in peripheral and central events separately whereas (d) shows the distributions integrated over $|\Delta\phi|<\pi/3$ and $|\Delta\phi|>2\pi/3$, and plotted as a function of the $\sum E_{\mathrm{T}}^{\mathrm{Pb}}$, the sum of transverse energy measured in the FCal in the z-direction of the lead beam. Both the near-side and away-side yield show a similar variation as a function of $\sum E_{\mathrm{T}}^{\mathrm{Pb}}$ indicating that the ridge has a near and away-side component. To further investigate the connection between the near-side and away-side, the $Y(\Delta\phi)$ distributions for peripheral and central events are shown in Fig. 16 (right) in various p_{T}^{a} ranges with $0.5<p_{\mathrm{T}}^{b}<4$ GeV together with a fit to the function $a_0+2a_2\cos(2\Delta\phi)$. The relative amplitude of the $\cos(2\Delta\phi)$ modulation of $\Delta Y(\phi)$, c_2, can be estimated using a_0, a_2, and the extracted value of b_{ZYAM} for central events as $c_2\equiv a_2/(b^{\mathrm{C}}_{\mathrm{ZYAM}}+a_0)$. Figure 17 (left) coefficient in lead-lead collisions is shown on the right [47]. It can be seen that the modulation parameter has a similar p_{T} dependence in both proton-lead and lead-lead collisions where this effect is usually attributed to the collective expansion of the medium.

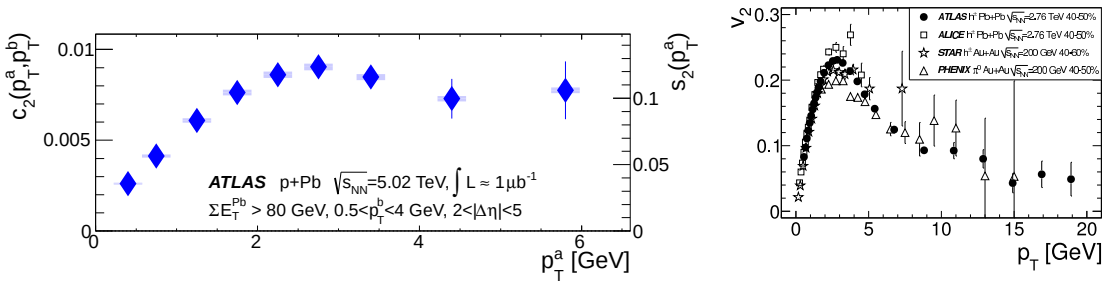

Figure 17: (left) p_{T} dependence of c_2 (left axis) and s_2 (right axis). The right axis differs from the left only by a multiplicative factor $1/\sqrt{5.4\times10^{-3}}$ (see [46]). The error bars and shaded boxes represent the statistical and systematic uncertainties, respectively. (right) For comparison, the second harmonic Fourier coefficient v_2 in lead-lead collisions in the 40-50% centrality interval from various experiments [47].

References

[1] **ATLAS** Collaboration, *The ATLAS Experiment at the CERN Large Hadron Collider*, *JINST* **3** (2008) S08003.

[2] L. Evans and P. Bryant, *LHC Machine*, *JINST* **3** (2008) S08001.

[3] **ATLAS** Collaboration, *The ATLAS Inner Detector commissioning and calibration*, *Eur. Phys. J.* **C 70** (2010) 787–821, [arXiv:1004.5293].

[4] **ATLAS** Collaboration, *Readiness of the ATLAS Liquid Argon Calorimeter for LHC Collisions*, *Eur. Phys. J.* **C 70** (2010) 723–753, [arXiv:0912.2642].

[5] **ATLAS** Collaboration, *Readiness of the ATLAS Tile Calorimeter for LHC collisions*, *Eur. Phys. J.* **C 70** (2010) 1193–1236, [arXiv:1007.5423].

[6] **ATLAS** Collaboration, *Commissioning of the ATLAS Muon Spectrometer with Cosmic Rays*, *Eur. Phys. J.* **C 70** (2010) 875–916, [arXiv:1006.4384].

[7] **ATLAS** Collaboration, *Performance of the ATLAS Trigger System in 2010*, *Eur. Phys. J.* **C72** (2012) 1849, [arXiv:1110.1530].

[8] https://twiki.cern.ch/twiki/bin/view/AtlasPublic/CombinedSummaryPlots.

[9] **ATLAS** Collaboration, *Statistical combination of top quark pair production cross-section measurements using dilepton, single-lepton, and all-hadronic final states at* $\sqrt{s} = 7$ TeV *with the ATLAS detector*, ATLAS-CONF-2012-024.

[10] **ATLAS** Collaboration, *Measurement of the top quark pair production cross-section with ATLAS in pp collisions at* $\sqrt{s} = 7$ *TeV in the single-lepton channel using semileptonic b decays*, ATLAS-CONF-2012-131.

[11] **ATLAS** Collaboration, *Measurement of the* $t\bar{t}$ *production cross section in the tau+jets channel using the ATLAS detector*, *Eur.Phys.J.* **C73** (2013) 2328, [arXiv:1211.7205].

[12] **ATLAS** Collaboration, *Measurement of the top quark pair cross section with ATLAS in pp collisions at* $\sqrt{s} = 7$ TeV *using final states with an electron or a muon and a hadronically decaying* τ *lepton*, *Phys.Lett.* **B717** (2012) 89–108, [arXiv:1205.2067].

[13] **ATLAS** Collaboration, *Measurement of the* $t\bar{t}$ *production cross section in the all-hadronic channel in ATLAS with* $\sqrt{s} = 7$ *TeV data*, ATLAS-CONF-2012-031.

[14] **ATLAS** Collaboration, *Measurement of the top quark pair production cross section in the single-lepton channel with ATLAS in proton-proton collisions at 8 TeV using kinematic fits with b-tagging*, ATLAS-CONF-2012-149.

[15] **ATLAS** Collaboration, *Measurement of the top quark pair production cross-section with ATLAS in the single lepton channel*, *Phys. Lett.* **B711** (2012) 244–263, [arXiv:1201.1889].

[16] M. Aliev, H. Lacker, U. Langenfeld, S. Moch, P. Uwer, et al., *HATHOR: HAdronic Top and Heavy quarks crOss section calculatoR*, *Comput.Phys.Commun.* **182** (2011) 1034–1046, [arXiv:1007.1327].

[17] **ATLAS** Collaboration, *Measurement of ZZ production in pp collisions at* $\sqrt{s} = 7$ TeV *and limits on anomalous ZZZ and ZZgamma couplings with the ATLAS detector*, CERN-PH-EP-2012-318, [arXiv:1211.6096].

[18] **ATLAS** Collaboration, *Measurement of the total ZZ production cross section in the four-lepton channel using* $5.8\,fb^{-1}$ *of ATLAS data at* $\sqrt{s}$ *= 8 TeV*, ATLAS-CONF-2012-090.

[19] **ATLAS** Collaboration, *Observation of a new particle in the search for the Standard Model Higgs boson with the ATLAS detector at the LHC*, *Phys.Lett.* **B716** (2012) 1–29, [arXiv:1207.7214].

[20] **CMS** Collaboration, *Observation of a new boson at a mass of 125 GeV with the CMS experiment at the LHC*, *Phys.Lett.* **B716** (2012) 30–61, [arXiv:1207.7235].

[21] **ATLAS** Collaboration, *Search for the Standard Model Higgs boson in* $H \to \tau\tau$ *decays in proton-proton collisions with the ATLAS detector*, ATLAS-CONF-2012-160.

[22] **ATLAS** Collaboration, *Search for the Standard Model Higgs boson in produced in association with a vector boson and decaying to bottom quarks with the ATLAS detector*, ATLAS-CONF-2012-161.

[23] **ATLAS** Collaboration, *Update of the* $H \to WW^{(*)} \to e\nu\mu\nu$ *Analysis with 13* fb^{-1} *of* $\sqrt{s} = 8$ *TeV Data Collected with the ATLAS Detector*, ATLAS-CONF-2012-158.

[24] **ATLAS** Collaboration, *Observation and study of the Higgs boson candidate in the two photon decay channel with the ATLAS detector at the LHC*, ATLAS-CONF-2012-168.

[25] **ATLAS** Collaboration, *Observation of an excess of events in the search for the Standard Model Higgs boson in the gamma-gamma channel with the ATLAS detector*, ATLAS-CONF-2012-091.

[26] **ATLAS** Collaboration, *Observation of an excess of events in the search for the Standard Model Higgs boson in the* $H \to ZZ^{(*)} \to 4\ell$ *channel with the ATLAS detector*, ATLAS-CONF-2012-169.

[27] **ATLAS** Collaboration, *An update of combined measurements of the new higgs-like boson with high mass resolution channels*, .

[28] **ATLAS** Collaboration, *Search for squarks and gluinos with the ATLAS detector using final states with jets and missing transverse momentum and 5.8* fb^{-1} *of* $\sqrt{s}$*=8 TeV proton-proton collision data*, ATLAS-CONF-2012-109.

[29] **ATLAS** Collaboration, *Search for supersymmetry at* $\sqrt{s} = 8$ TeV *in final states with jets, missing transverse momentum and one isolated lepton*, ATLAS-CONF-2012-104.

[30] **ATLAS** Collaboration, *Search for direct sbottom production in event with two b-jets using* $12.8\,fb^{-1}$ *of pp collisions at* $\sqrt{s} = 8$ TeV *with the ATLAS Detector*, ATLAS-CONF-2012-165.

[31] D. R. Tovey, *On measuring the masses of pair-produced semi-invisibly decaying particles at hadron colliders*, *JHEP* **0804** (2008) 034, [arXiv:0802.2879].

[32] **ATLAS** Collaboration, *Search for a supersymmetric top-quark partner in final states with two leptons in $\sqrt{s} = 8$ TeV pp collisions using 13 fb^{-1} of ATLAS data*, ATLAS-CONF-2012-167.

[33] **ATLAS** Collaboration, *Search for direct top squark pair production in final states with one isolated lepton, jets, and missing transverse momentum in $\sqrt{s} = 8$ TeV pp collisions using 13.0 fb^{-1} of ATLAS data*, ATLAS-CONF-2012-166.

[34] **ATLAS** Collaboration, *Search for direct stop production in events with missing transverse momentum and two b-jets using 12.8 fb^{-1} of pp collisions at $\sqrt{s} = 8$ TeV with the ATLAS detector*, ATLAS-CONF-2013-001.

[35] **ATLAS** Collaboration, *Search for a supersymmetric partner to the top quark in final states with jets and missing transverse momentum at $\sqrt{s} = 7$ TeV with the ATLAS detector*, CERN-PH-EP-2012-201, [arXiv:1208.1447].

[36] **ATLAS** Collaboration, *Search for direct top squark pair production in final states with one isolated lepton, jets, and missing transverse momentum in $\sqrt{s} = 7$ TeV pp collisions using 4.7 fb^{-1} of ATLAS data*, *Phys.Rev.Lett.* (2012) CERN-PH-EP-2012-200, [arXiv:1208.2590].

[37] **ATLAS** Collaboration, *Search for a heavy top-quark partner in final states with two leptons with the ATLAS detector at the LHC*, *JHEP* **1211** (2012) 094, [arXiv:1209.4186].

[38] **ATLAS** Collaboration, *Search for light scalar top quark pair production in final states with two leptons with the ATLAS detector in $\sqrt{s} = 7$ TeV proton-proton collisions*, *Eur.Phys.J.* **C72** (2012) 2237, [arXiv:1208.4305].

[39] **ATLAS** Collaboration, *Search for light top squark pair production in final states with leptons and b^- jets with the ATLAS detector in $\sqrt{s} = 7$ TeV proton-proton collisions*, *Phys.Lett.* **B720** (2013) 13–31, [arXiv:1209.2102].

[40] **ATLAS** Collaboration, *Measurement of Z boson Production in Pb+Pb Collisions at $\sqrt{s_{NN}} = 2.76$ TeV with the ATLAS Detector*, *Phys.Rev.Lett.* **110** (2013) 022301, [arXiv:1210.6486].

[41] **ATLAS** Collaboration, *Measurement of momentum imbalance in $Z \to \ell\ell$ + Jet events in Lead-Lead collisions at $\sqrt{s_{NN}}$= 2.76 TeV with the ATLAS detector*, ATLAS-CONF-2012-119.

[42] M. Cacciari, G. P. Salam, and G. Soyez, *The anti-k_t jet clustering algorithm*, *JHEP* **04** (2008) 063, [arXiv:0802.1189].

[43] **ATLAS** Collaboration, *Centrality dependence of Jet Yields and Jet Fragmentation in Lead-Lead Collisions at $\sqrt{s_{NN}} = 2.76$ TeV with the ATLAS detector at the LHC*, ATLAS-CONF-2011-075.

[44] **ATLAS** Collaboration, *Measurement of the centrality dependence of open heavy flavour production in lead-lead collisions at sqrts = 2.76 TeV with the ATLAS detector*, ATLAS-CONF-2012-050.

[45] **CMS** Collaboration, *Observation of Long-Range Near-Side Angular Correlations in Proton-Proton Collisions at the LHC*, *JHEP* **1009** (2010) 091, [arXiv:1009.4122].

[46] **ATLAS** Collaboration, *Observation of Associated Near-side and Away-side Long-range Correlations in $\sqrt{s_{NN}} = 5.02$ TeV Proton-lead Collisions with the ATLAS Detector*, CERN-PH-EP-2012-366, [arXiv:1212.5198].

[47] **ATLAS** Collaboration, *Measurement of the pseudorapidity and transverse momentum dependence of the elliptic flow of charged particles in lead-lead collisions at $\sqrt{s_{NN}} = 2.76$ TeV with the ATLAS detector*, *Phys.Lett.* **B707** (2012) 330–348, [arXiv:1108.6018].